Optical Properties of the Infinite-Layer math xmlns="http://www.w3.org/1998/Math/MathML" display="inline">mrow>msub>mrow>mi>La/mi>/mrow> mrow>mn>1/mn>mo>−/mo>mi>x/mi>/mrow>/msub>m sub>mrow>mi>Sr/mi>/mrow>mrow>mi>x/mi>/mrow>/m sub>msub>mrow>mi>NiO/mi>/mrow>mrow>mn>2/mn>/ mrow>/msub>/mrow>/math> and Hidden Hund's Physics

Chang-Jong Kang and Gabriel Kotliar

Phys. Rev. Lett. **126**, 127401 — Published 22 March 2021

DOI: 10.1103/PhysRevLett.126.127401

Optical properties of the infinite-layer $La_{1-x}Sr_xNiO_2$ and hidden Hund's physics

Chang-Jong Kang[1] and Gabriel Kotliar[1,2]

[1] *Department of Physics and Astronomy, Rutgers University, Piscataway, New Jersey 08856, USA*
[2] *Department of Condensed Matter Physics and Materials Science, Brookhaven National Laboratory, Upton, New York 11973, USA*

(Dated: January 4, 2021)

We investigate the optical properties of the normal state of the infinite-layer $La_{1-x}Sr_xNiO_2$ using DFT+DMFT. We find a correlated metal which exhibits substantial transfer of spectral weight to high energies relative to the density functional theory. The correlations are not due to Mott physics, which would suppress the charge fluctuations and the integrated optical spectral weight as we approach a putative insulating state. Instead we find the unusual situation, that the integrated optical spectral weight *decreases* with doping and *increases* with increasing temperature. We contrast this with the coherent component of the optical conductivity, which *decreases* with increasing temperature as a result of a coherence−incoherence crossover. Our studies reveal that the effective crystal field splitting is dynamical and increases strongly at low frequency. This leads to a picture of a Hund's metallic state, where dynamical orbital fluctuations are visible at intermediate energies, while at low energies a Fermi surface with primarily $d_{x^2-y^2}$ character emerges. The infinite-layer nickelates are thus in an intermediate position between the iron based high temperature superconductors where multiorbital Hund's physics dominates, and a one-band system such as the cuprates. To capture this physics we propose a low-energy two-band model with atom centered e_g states.

Introduction— The recent discovery of superconductivity in the infinite-layer nickelates, $Nd_{1-x}Sr_xNiO_2$ [1], has attracted intensive interests due to material similarities with high-T_c cuprate superconductors. Several follow-up experiments confirmed the superconductivity [2–6], with some possibly contradictory observations [7, 8]. Nomura *et al.* estimated the electron-phonon coupling mediated T_c to be ~ 0.1 K [17], much less than the observed $T_c \approx 15$ K, showing the mechanism for superconductivity is unconventional thus electron correlations play an important role.

There are many experimental investigations into the infinite-layer nickelates [1–16] and multiple theoretical techniques have been applied to study their electronic structure [17–27, 29–49]. On the theory side, three different views of these materials are emerging. In the first one, the infinite-layer nickelate has a cuprate-like correlated $d_{x^2-y^2}$ band near a Mott transition and an additional uncorrelated "spectator" band near the Fermi level which provides self-doping and is supported by density functional theory (DFT) [17–21], DFT plus dynamical mean-field theory (DFT+DMFT) [22–24], and model calculations [21, 25, 26]. The second suggests that multiorbital effects are important as for example Hund's physics, using DFT+DMFT [27], GW+DMFT [28, 29], and model studies [30–33]. A third approach invokes Kondo physics between correlated and uncorrelated bands. This is supported by DFT [34], DFT+Gutzwiller [35], DFT+DMFT [35, 36], and model calculations [37, 38]. In this paper we present a fourth perspective, incorporating ideas from the first two viewpoints. Here frequency renormalization of the crystal fields plays a major role and results in Hund's multiorbital physics present at intermediate energies, but hidden at low energies. This is a new prototype for a strongly correlated metal.

To reach this conclusion we perform fully charge self-consistent DFT+DMFT calculations [50–53] implemented in the all-electron full-potential Wien2k package [54] with the exact double counting scheme [55] (see computational details in Supplementary Material (SM) [56]). This approach was recently shown to give results consistent with the occupancies measured in high-energy spectroscopies [14, 27, 29]. Here we focus on the basic electronic structure of the infinite-layer nickelates to extract the basic physics of this class of compounds. We give special attention to the optical conductivity. Experiments in this were crucial in identifying early on the origin and nature of electronic correlations in different archetypical systems [57].

Results: Optical Conductivity— The DFT+DMFT optical conductivity is computed with the formalism presented in Refs. [53, 56] and is shown in Fig. 1 with the DFT reference provided for comparison. The optical conductivity consists of a Drude weight and interband transitions at ∼3.5, ∼6, and ∼8.5 eV. The former corresponds to a transition from Ni $3d$ to La $4f$ orbitals and the last two correspond to transitions from O $2p$ to La $4f$ orbitals [56].

The temperature(T)-dependent optical conductivity is displayed in Fig. 2(a). The Drude peak develops gradually upon cooling, resulting in a decrease of the resistivity ρ as shown in the inset of Fig. 2(a). The computed ρ follows a T^2 behavior, found experimentally at intermediate temperatures [12]. At lower temperatures a resistivity upturn below $T \sim 100$ K is observed in experiments [1, 12, 13] which we ascribe to disorder effects which are not included in the calculations.

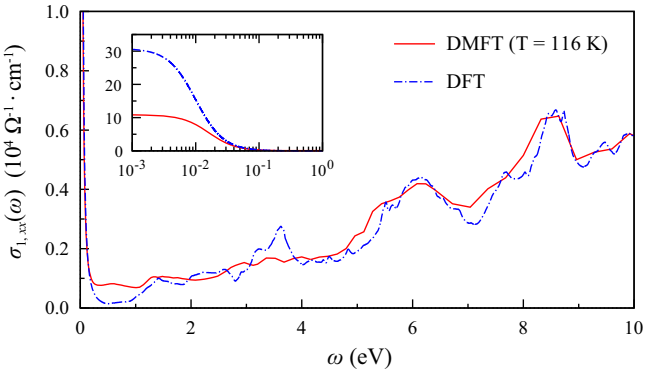

FIG. 1. Optical conductivity of $LaNiO_2$ in a broad ω frequency range computed within both DFT and DFT+DMFT methods. The inset is provided to magnify the Drude weight.

Results: Integrated Optical Spectral Weight— To understand the physics of this material we analyze the integrated spectral weight $K(\Omega) = \int_0^{\Omega} \sigma_1(\omega) d\omega$ as a function of the cutoff frequency Ω [57]. Figure 2(b) displays $K(\Omega)$ for DMFT normalized to the DFT Drude weight. The ratio of $K_{\rm DMFT}(\Omega)/K_{\rm DFT}$ decreases upon heating for low cutoff Ω (less than ∼50 meV) as a result of the broadening of the Drude peak. Above this cutoff, the integrated spectral weight increases with increasing temperature. The integrated spectral weight up to Ω_c = 0.369 eV (chosen to exclude a contribution from interband transitions) in DMFT is about 0.6 of the DFT value at $T = 116$ K. Part of the lost weight in the Drude peak is transferred to a low-energy interband transition around ∼0.5 eV as shown in Fig. 1.

The reduction of $K_{\rm DMFT}/K_{\rm DFT}$ depicted in Fig. 2(b) demonstrates the significance of electronic correlations which reduces the electronic kinetic energy. For $LaNiO_2$, $K_{\rm DMFT}/K_{\rm DFT} = 0.5 - 0.6$ at Ω_c, thereby suggesting that it is a (moderately) correlated metal. The kinetic energy ratio is comparable to Hund metal compounds such as LaFePO and $SrRuO_3$ [57]. It is noteworthy that $K_{\rm DMFT}/K_{\rm DFT} \approx 0$ for cuprates of La_2CuO_2 and Nd_2CuO_4, those are charge-transfer insulators, and ∼0.2 for $La_{2-x}Sr_xCuO_2$ (x = 0.1, 0.15, 0.2) [58]. In addition, in the paramagnetic metallic phase of V_2O_3, which ia a prototypical Mott system, $K_{\rm DMFT}/K_{\rm DFT} \approx 0.2$ [57]. Based on the values of $K_{\rm DMFT}/K_{\rm DFT}$, $LaNiO_2$ is far from a Mott system, but close to a Hund's metal.

Notice that the behavior of $K_{\rm DMFT}/K_{\rm DFT}$ of $LaNiO_2$ as a function of temperature (when Ω is large) is the *opposite* of what is observed in canonical Mott insulating systems such as V_2O_3 where $K_{\rm DMFT}(\Omega)$ (or $K_{\rm DMFT}/K_{\rm DFT}$) decreases upon heating (within the paramagnetic metallic phase) [59] (see details in SM [56]). This reflects the fact that the kinetic energy is reduced as an insulating state is approached at higher temperatures. Therefore, $LaNiO_2$ is far from a Mott system and closer to a Hund's system such as $BaFe_2As_2$ [74, 75].

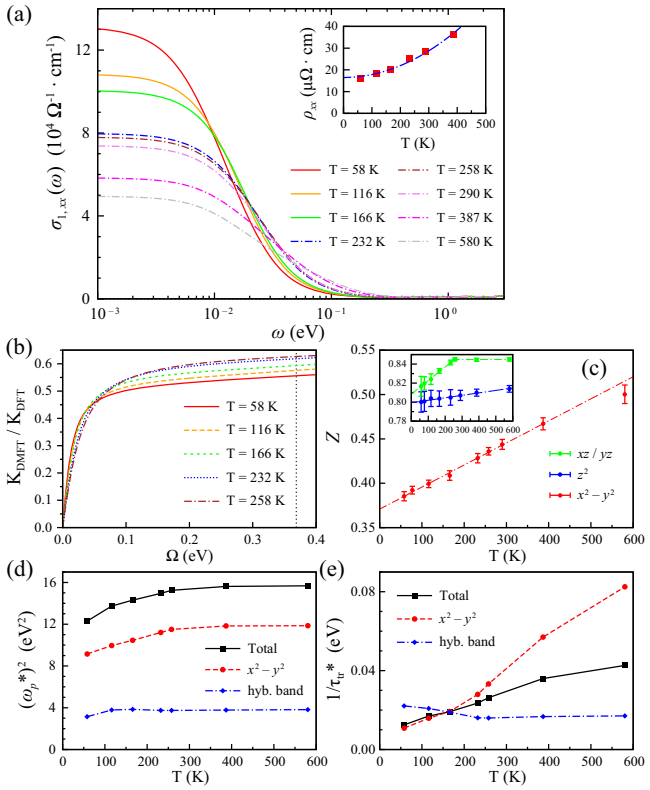

FIG. 2. (a) Temperature-dependent optical conductivity of $LaNiO_2$ calculated within DFT+DMFT. The ω-axis is presented in a logarithmic scale. The calculated resistivity provided in the inset shows the T^2 behavior. The blue dash-dotted line in the inset is a guide for the eye by fitting ρ_{xx} to a parabolic function. (b) The kinetic energy ratio $K_{\rm DMFT}(\Omega)/K_{\rm DFT}$ as a function of integration cutoff value Ω provided for several temperatures. The vertical dotted line is the kinetic energy integration cutoff $\Omega_c = 0.369$ eV chosen to exclude a contribution from interband transitions. (c) Quasiparticle weight Z for Ni $d_{x^2-y^2}$, d_{z^2}, and d_{xz}/d_{yz} orbitals as a function of temperature. Error bars originate from the statistical errors in CTQMC simulations. The dash-dotted lines in (c) are guides for the eye by fitting Z to a linear function. (d) The effective plasma frequency square $(\omega_p^*)^2$ and (e) the effective quasiparticle scattering rate $1/\tau_{\rm tr}^*$ extracted from the computed optical conductivity within DFT+DMFT by using the formalism in Ref. [59].

Results: Orbital Character— We now turn to the orbital character of the different contribution to the optical features. First we analyze the quasiparticle weight Z as a function of T as depicted in Fig. 2(c) [76]. Ni $d_{x^2-y^2}$ has the smallest Z which is drastically smaller than the other $3d$ orbitals having $Z \approx 0.8$. Notice the strong temperature dependence of Z which increases linearly upon heating, a clear correlation effect, which implies the temperature dependence of the effective mass of the resilient quasiparticles [77, 78]. In contrast, the other orbitals have very weak or no temperature dependence as shown in the inset of Fig. 2(c). Hence, strong differentiation

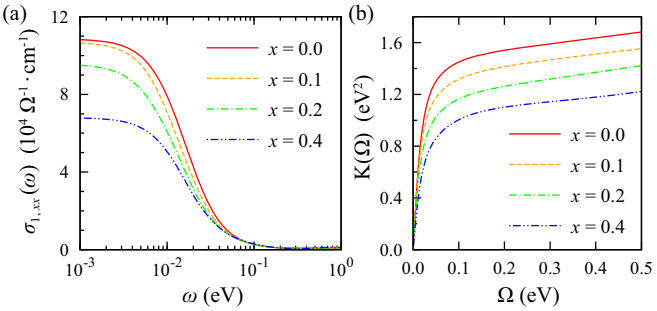

FIG. 3. (a) Doping-concentration-dependent optical conductivity of $La_{1-x}Sr_xNiO_2$ calculated within DFT+DMFT at $T = 116$ K. (b) The integrated optical spectral weight $K(\Omega)$ as a function of cutoff frequency Ω provided for several doping concentration x.

between the correlated $d_{x^2-y^2}$ band and an uncorrelated band with different orbital characters is present in this system.

The Drude peak could be decomposed into two characters: the correlated Ni $d_{x^2-y^2}$ and an uncorrelated hybridized band which includes Ni d_{z^2} and d_{xz}/d_{yz} orbitals [56]. It illustrates the multiorbital feature of $LaNiO_2$. The dominant component of the Drude peak is the correlated $d_{x^2-y^2}$ which exhibits strong temperature dependence as shown in Z. The remaining contribution originates from the uncorrelated hybridized band that are almost temperature independent. Therefore, T-dependent width of the Drude peak is almost solely determined by the electronic correlation exhibited in the $d_{x^2-y^2}$ band.

To gain more insight into the physics of the infinite-layer $LaNiO_2$, we perform a low-energy extended Drude analysis to extract the effective plasma frequency ω_p^* and quasiparticle scattering rate $1/\tau_{\rm tr}^*$ from the computed optical conductivity [59]. In the multiband situation it is useful to decompose the Drude peak into two contributions, one coming from the correlated $d_{x^2-y^2}$ and the second from the uncorrelated hybridized band. The dc conductivity, therefore, can be written as a sum of the two contributions: $\sigma = \sum_i (\omega_{p,i}^*)^2 \tau_{{\rm tr},i}^*/4\pi$, where i is a band index. Figures 2(d) and (e) show $(\omega_p^*)^2$ and $1/\tau_{\rm tr}^*$ for each band component as a function of temperature. The uncorrelated hybridized band shows almost temperature independent $(\omega_p^*)^2$ and $1/\tau_{\rm tr}^*$. In contrast, $(\omega_p^*)^2$ for $d_{x^2-y^2}$ shows a linear temperature dependence up to $T \sim 300$ K where it saturates at the coherence-incoherence crossover, and was also observed in ruthenates [79] (see Section XII in SM [56]). The temperature dependence in $(\omega_p^*)^2$ can be related to the temperature dependence of Z discussed above. The quasiparticle lifetime $1/\tau_{\rm tr}^*$ for $d_{x^2-y^2}$ is approximately parabolic in temperature below the coherent temperature and shows a deviation from the quadratic behavior above the coherence-incoherence crossover temperature.

Results: Doping Dependence— Now, we turn our attention to Sr-doped $LaNiO_2$, where Sr doping provides holes to $LaNiO_2$. Figure 3(a) shows the doping-concentration(x)-dependent optical conductivity of $La_{1-x}Sr_xNiO_2$. The Drude peak and the integrated optical spectral weight $K(\Omega)$ decrease with increasing doping as depicted in Fig. 3. Since $K(\Omega)$ is proportional to the electronic kinetic energy, it indicates the *decrease* of the kinetic energy upon doping. This behavior is the opposite of what is observed in a Mott system where doping increases the electronic kinetic energy [57, 80]. This provides further evidence of that $La_{1-x}Sr_xNiO_2$ is far from a Mott transition. Mott-like behavior was reported in recent GW+DMFT calculations [29].

The decrease in the kinetic energy originates from the fact that the low-energy carrier number, n_e, defined by the volume of the Fermi surface, decreases upon doping as presented in Table I. Note that two distinct charge carriers are realized in the Fermi surface, those are the correlated Ni $d_{x^2-y^2}$ and the uncorrelated hybridized band with Ni d_{z^2} (see Fig. 4). n_e for $d_{x^2-y^2}$ decreases significantly upon doping while n_e for the uncorrelated hybridized band is small and varies less. From the perspective of n_e, the doped holes mostly go to the $d_{x^2-y^2}$ band [81].

It is important to distinguish the high-energy d occupancy, which is measured in x-ray spectroscopy [14] and has been shown to be independent of doping [27], from the low-energy occupancy n_e that decreases with increasing hole doping. This effect, which competes with an increase in Z with increasing hole doping [27], dominates the behavior of the kinetic energy.

Results: Electronic Structure— The dependence of the k-resolved spectral function with doping is shown in Fig. 4(a). The dominant character at the Fermi level $E_{\rm F}$ is $d_{x^2-y^2}$ and gives a large Fermi surface (FS) shown in Fig. 4(b). The uncorrelated hybridized band gives small FSs at Γ and A. Hence, the multiorbital character is clearly seen in the calculations as noticed in earlier works [27, 29, 31].

At $x = 0.2$, the hybridized band with Ni d_{z^2} detaches from $E_{\rm F}$. As a result, the FS at Γ disappears. Upon further doping, at $x = 0.5$, another FS from the hybridized band detaches from $E_{\rm F}$ as well and the FS from Ni $d_{x^2-y^2}$ is solely realized. Therefore, two distinct Lifshitz transi-

TABLE I. The low-energy carrier number, n_e, as a function of doping ratio. n_e is defined by the volume of the Fermi surface. 3-dimensional Fermi surface computed with DFT+DMFT is presented in Supplemental Material [56].

	$x = 0.0$	$x = 0.1$	$x = 0.2$	$x = 0.3$	$x = 0.4$	$x = 0.5$
Ni $d_{x^2-y^2}$	0.98	0.93	0.85	0.76	0.66	0.56
Hybridized band	0.07	0.03	0.02	0.01	∼0.00	0.00

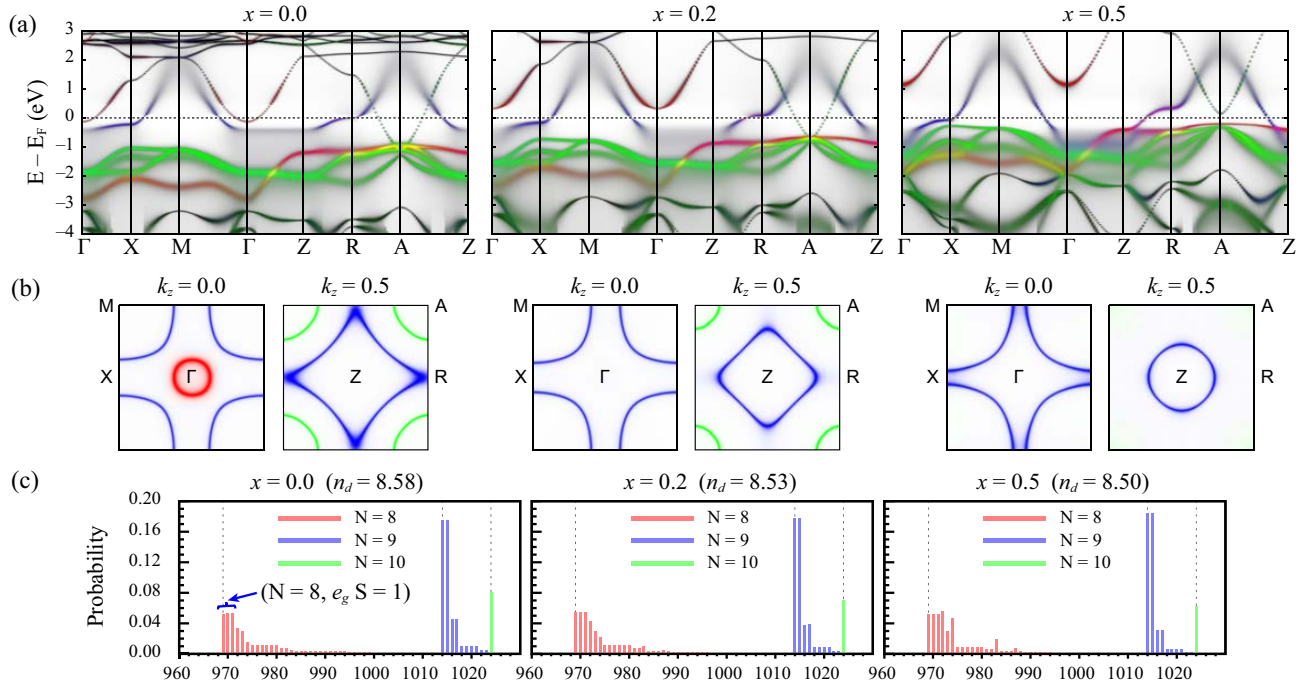

FIG. 4. Electronic structures of $La_{1-x}Sr_xNiO_2$ computed within DFT+DMFT at $T = 116$ K. (a) k-resolved spectral functions. (b) Fermi surfaces of $La_{1-x}Sr_xNiO_2$ at $k_z = 0.0$ and $k_z = 0.5$ planes. Ni d_{z^2}, $d_{x^2-y^2}$, and t_{2g} (d_{xz}/d_{yz}) orbital characters are presented by red, blue, and green, respectively, in (a) (in (b)). (c) The DMFT valence histogram of the Ni-3d shell is provided for $x =$ (left) 0.0, (middle) 0.2, and (right) 0.5. The 1024 possible atomic configurations are sorted by the number of 3d electrons of the individual configuration.

tions are realized upon doping [27, 42].

Results: Two-Band Model— The multiorbital character is definitely seen in the DMFT valence histogram as depicted in Fig. 4(c), where the second largest probability of 0.16 comes from the atomic configuration of ($N = 8$, e_g $S = 1$) with a spin-triplet state within Ni e_g states [82]. Note that ($N = 9$, $S = 1/2$) with one hole in Ni $d_{x^2-y^2}$ has the largest probability of 0.35. These two largest probabilities are nearly constant over the doping concentration. Since the FS has primarily Ni $d_{x^2-y^2}$, one could interpret in a one-band scenario as a low-energy model [21, 24]. However we find that Hund's coupling J_H decreases Z and increases $-\mathrm{Im}\Sigma(i0^+)$ for $d_{x^2-y^2}$ (see Fig. S14 in SM [56]), which is surprising as the atomic ground state configuration has one hole. This J_H dependence of the correlation strength is the hallmark of a Hund's metal [68, 83, 84]. This is because a metallic state requires fluctuations between d^9 and d^8, and J_H is important in the latter configuration as seen clearly in the valence histogram in Fig. 4(c). We can think of the crystal field as being frequency dependent, at low energies it leaves $d_{x^2-y^2}$ as the most active orbital, but at intermediate frequencies both $d_{x^2-y^2}$ and d_{z^2} are important (see Section XIV and Fig. S17 in SM [56]). Therefore, the infinite-layer nickelate is a Hund's metal where Hund's correlation is hidden at low energies but noticeable at intermediate energies. It is different from the Hund's metal realized in iron pnictides, chalcogenides, and ruthenates, where a configuration with more than one electron or hole, makes Hund's correlation prominent in the atomic ground state configuration. This is made explicit by a two-band Wannier construction which is atom centered with the symmetry of the two Ni e_g orbitals, but which exhibits the clear difference of $d_{x^2-y^2}$ and d_{z^2} provided in SM (see Section XIII and Fig. S16 in SM [56]) which is different from alternative low-energy Wannier constructions reported before [14, 17, 34–36, 43, 44]. This perspective provides a qualitative understanding of the variation of the Hall coefficient with doping and temperature which is seen in the experiments [1, 4, 5] as discussed in SM [56].

Conclusion— To summarize, we have computed the basic electronic structure of the normal state of $La_{1-x}Sr_xNiO_2$ within DFT+DMFT with a focus on the temperature and doping dependence of the optical conductivity. We find signs of strong correlations in the optical response as the ratio of the optical spectral weight to the DFT band theory (i.e. $K_{\mathrm{DMFT}}/K_{\mathrm{DFT}}$) is small (this can be a feature of Mott or Hund's systems). We find that the evolutions of the optical spectral weight with (i) temperature and (ii) doping are qualitatively different from those in a canonical Mott-Hubbard system and more similar to those of an orbitally differentiated Hund's metal with a highly correlated $d_{x^2-y^2}$ and a d_{z^2} orbital

with weaker correlations. To reveal the basic physics that govern these materials we studied the dependence of the physical quantities on the interaction parameters. We find (1) DMFT valence histogram with enhanced high spin occupation and (2) strong dependence of the coherence scale with Hund's coupling J_H, both are clear signatures of the Hund's metal. This type of material is quite unique since Hund's physics is hidden at low energies due to the large crystal field splitting but noticeable at intermediate energies where the (dynamical) crystal field splitting becomes small and Hund's coupling dominates. It is in an intermediate position between the multiorbital iron based superconductors and one-band high-T_c cuprate superconductors, thus opening a new research area in the theory of correlated materials.

Acknowledgment— We are grateful to K. Haule, M. Kim, S. Choi, Y. Wang, H. Miao, and G. L. Pascut for useful discussions. C.-J. K. and G. K. were supported by the U.S. Department of Energy, Office of Science, Basic Energy Sciences as a part of the Computational Materials Science Program through the Center for Computational Design of Functional Strongly Correlated Materials and Theoretical Spectroscopy.

[1] Danfeng Li, Kyuho Lee, Bai Yang Wang, Motoki Osada, Samuel Crossley, Hye Ryoung Lee, Yi Cui, Yasuyuki Hikita, and Harold Y. Hwang, "Superconductivity in an infinite-layer nickelate," Nature **572**, 624 (2019).

[2] Kyuho Lee, Berit H. Goodge, Danfeng Li, Motoki Osada, Bai Yang Wang, Yi Cui, Lena F. Kourkoutis, and Harold Y. Hwang, "Aspects of the synthesis of thin film superconducting infinite-layer nickelates," APL Materials **8**, 041107 (2020).

[3] Motoki Osada, Bai Yang Wang, Berit H. Goodge, Kyuho Lee, Hyeok Yoon, Keita Sakuma, Danfeng Li, Masashi Miura, Lena F. Kourkoutis, and Harold Y. Hwang, "A superconducting praseodymium nickelate with infinite layer structure," Nano Lett. **20**, 5735 (2020).

[4] Shengwei Zeng, Chi Sin Tang, Xinmao Yin, Cgangjian Li, Zhen Huang, Junxiong Hu, Wei Liu, Ganesh Ji Omar, Hariom Jani, Zhi Shiuh Lim, Kun Han, Dongyang Wan, Ping Yang, Andrew T. S. Wee, Ariando Ariando, "Phase diagram and superconducting dome of infinte-layer $Nd_{1-x}Sr_xNiO_2$ thin films," Phys. Rev. Lett. **125**, 147003 (2020).

[5] Danfeng Li, Bai Yang Wang, Kyuho Lee, Shannon P. Harvey, Motoki Osada, Berit H. Goodge, Lena F. Kourkoutis, Harold Y. Hwang, "Superconducting Dome in $Nd_{1-x}Sr_xNiO_2$ Infinite Layer Films," Phys. Rev. Lett. **125**, 027001 (2020).

[6] Qiangqiang Gu, Yueying Li, Siyuan Wan, Huazhou Li, Wei Guo, Huan Yang, Qing Li, Xiyu Zhu, Xiaoqing Pan, Yuefeng Nie, and Hai-Hu Wen, "Single particle tunneling spectrum of superconducting $Nd_{1-x}Sr_xNiO_2$ thin films," Nat. Commun. **11**, 6027 (2020).

[7] Qing Li, Chengping He, Jin Si, Xiyu Zhu, and Hai-Hu Wen, "Absence of superconductivity in bulk $Nd_{1-x}Sr_xNiO_2$," Communications Materials **1**, 16 (2020).

[8] Xiao-Rong Zhou, Ze-Xin Feng, Pei-Xin Qin, Han Yan, Shuai Hu, Hui-Xin Guo, Xiao-Ning Wang, Hao-Jiang Wu, Xin Zhang, Hong-Yu Chen, Xue-Peng Qiu, and Zhi-Qi Liu, "Absence of superconductivity in $Nd_{0.8}Sr_{0.2}NiO_x$ thin films without chemical reduction," Rare Metals **39**, 368 (2020).

[9] Michel Crespin, Pierre Levitz, and Lucien Gatineau, "Reduced forms of $LaNiO_3$ perovskite. Part 1.—Evidence for new phases: $La_2Ni_2O_5$ and $LaNiO_2$," J. Chem. Soc., Faraday Trans. 2 **79**, 1181 (1983).

[10] Pierre Levitz, Michel Crespin, and Lucien Gatineau, "Reduced forms of $LaNiO_3$ perovskite. Part 2.—X-ray structure of $LaNiO_2$ and extended X-ray absorption fine structure study: local environment of monovalent nickel," J. Chem. Soc., Faraday Trans. 2 **79**, 1195 (1983).

[11] M. A. Hayward, M. A. Green, M. J. Rosseinsky, and J. Sloan, "Sodium Hydride as a Powerful Reducing Agent for Topotactic Oxide Deintercalation: Synthesis and Characterization of the Nickel(I) Oxide $LaNiO_2$," J. Am. Chem. Soc. **121**, 8843 (1999).

[12] Ai Ikeda, Yoshihara Krockenberger, Hiroshi Irie, Michio Naito, and Hideki Yamamoto, "Direct observation of infinite NiO_2 planes in $LaNiO_2$ films," Applied Physics Express **9**, 061101 (2016).

[13] Ai Ikeda, Takaaki Manabe, Michio Naito, "Improved conductivity of infite-layer $LaNiO_2$ thin films by metal organic decomposition," Physica C **495**, 134 (2013).

[14] M. Hepting, D. Li, C. J. Jia, H. Lu, E. Paris, Y. Tseng, X. Feng, M. Osada, E. Been, Y. Hikita, Y.-D. Chuang, Z. Hussain, K. J. Zhou, A. Nag, M. Garcia-Fernandez, M. Rossi, H. Y. Huang, D. J. Huang, Z. X. Shen, T. Schmitt, H. Y. Hwang, B. Moritz, J. Zaanen, T. P. Devereaux, and W. S. Lee, "Electronic structure of the parent compound of superconducting infinite-layer nickelates," Nature Materials **19**, 381 (2020).

[15] Ying Fu, Le Wang, Hu Cheng, Shenghai Pei, Xuefeng Zhou, Jian Chen, Shaoheng Wang, Ran Zhao, Wenrui Jiang, Cai Liu, Mingyuan Huang, XinWei Wang, Yusheng Zhao, Dapeng Yu, Fei Ye, Shanmin Wang, Jia-Wei Mei, "Core-level x-ray photoemission and Raman spectroscopy studies on electronic structures in Mott-Hubbard type nickelate oxide $NdNiO_2$," arXiv:1911.03177 (2019).

[16] Berit H. Goodge, Danfeng Li, Motoki Osada, Bai Yang Wang, Kyuho Lee, George A. Sawatzky, Harold Y. Hwang, and Lena F. Korkoutis, "Doping evolution of the Mott-Hubbard landscape in infinite-layer nickelates," arXiv:2005.02847 (2020).

[17] Yusuke Nomura, Motoaki Hirayama, Terumasa Tadano, Yoshihide Yoshimoto, Kazuma Nakamura, and Ryotaro Arita, "Formation of a two-dimensional single-component correlated electron system and band engineering in the nickelate superconductor $NdNiO_2$," Phys. Rev. B **100**, 205138 (2019).

[18] K.-W. Lee and W. E. Pickett, "Infinite-layer $LaNiO_2$: Ni^{1+} is not Cu^{2+}," Phys. Rev. B **70**, 165109 (2004).

[19] A. S. Botana and M. R. Norman, "Similarities and Differences between $LaNiO_2$ and $CaCuO_2$ and Implications for Superconductivity," Phys. Rev. X **10**, 011024 (2020).

[20] Motoaki Hirayama, Terumasa Tadano, Yusuke Nomura, and Ryotaro Arita, "Materials design of dynamically stable d^9 layered nickelates," Phys. Rev. B **101**, 075107

(2020).
[21] Hu Zhang, Lipeng Jin, Shanmin Wang, Bin Xi, Xingqiang Shi, Fei Ye, and Jia-Wei Mei, "Effective Hamiltonian for nickelate oxides $Nd_{1-x}Sr_xNiO_2$," Phys. Rev. Research **2**, 013214 (2020).
[22] Frank Lechermann, "Late transition metal oxides with infinite-layer structure: Nickelates versus cuprates," Phys. Rev. B **101**, 081110(R) (2020).
[23] Jonathan Karp, Antia S. Botana, Michael R. Norman, Hyowon Park, Manuel Zingl, and Andrew Millis, "Many-Body Electronic Structure of $NdNiO_2$ and $CaCuO_2$," Phys. Rev. X **10**, 021061 (2020).
[24] Motoharu Kitatani, Liang Si, Oleg Janson, Ryotaro Arita, Zhicheng Zhong, Karsten Held, "Nickelate superconductors - a renaissance of the one-band Hubbard model," npj Quantum Mater. **5**, 59 (2020).
[25] Xianxin Wu, Domenico Di Sante, Tilman Schwemmer, Werner Hanke, Harold Y. Hwang, Srinivas Raghu, and Ronny Thomale, "Robust $d_{x^2-y^2}$-wave superconductivity of infinite-layer nickelates," Phys. Rev. B **101**, 060504(R) (2020).
[26] Mi Jiang, Mona Berciu, and George A. Sawatzky, "Critical Nature of the Ni Spin State in Doped $NdNiO_2$," Phys. Rev. Lett. **124**, 207004 (2020).
[27] Y. Wang, C.-J. Kang, H. Miao, G. Kotliar, "Hund's metal physics: from $SrNiO_2$ to $NdNiO_2$," Phys. Rev. B **102**, 161118(R) (2020).
[28] Byungkyun Kang, Corey Melnick, Patrick Semon, Gabriel Kotliar, Sangkook Choi, "Infinite-layer nickelates as Ni-eg Hund's metals," arXiv:2007.14610 (2020).
[29] Francesco Petocchi, Viktor Christiansson, Fredrik Nilsson, Ferdi Aryasetiawan, and Philipp Werner, "Normal state of $Nd_{1-x}Sr_xNiO_2$ from self-consistent GW+EDMFT," arXiv:2006.00394 (2020).
[30] Lun-Hui Hu and Congjun Wu, "Two-band model for magnetism and superconductivity in nickelates," Phys. Rev. Research **1**, 032046(R) (2019).
[31] Philipp Werner and Shintaro Hoshino, "Nickelate superconductors: Multiorbital nature and spin freezing," Phys. Rev. B **101**, 041104(R) (2020).
[32] Ya-Hui Zhang and Ashvin Vishwanath, "Type-II $t-J$ model in superconducting nickelate $Nd_{1-x}Sr_xNiO_2$," Phys. Rev. Research **2**, 023112 (2020).
[33] Jun Chang, Jize Zhao, Yang Ding, "Hund-Heisenberg model in superconducting infinite-layer nickelates," Phys. J. B **93**, 220 (2020).
[34] Emily Been, Wei-Sheng Lee, Harold Y. Hwang, Yi Cui, Jan Zaanen, Thomas Devereaux, Brian Moritz, Chunjing Jia, "Theory of Rare-earth Infinite Layer Nickelates," arXiv:2002.12300 (2020).
[35] Frank Lechermann, "Multiorbital Processes Rule the $Nd_{1-x}Sr_xNiO_2$ Normal State," Phys. Rev. X **10**, 041002 (2020).
[36] Yuhao Gu, Sichen Zhu, Xiaoxuan Wang, Jiangping Hu, and Hanghui Chen, "A substantial hybridization between correlated Ni-d orbital and itinerant electrons in infinite-layer nickelates," Communications Physics **3**, 84 (2020).
[37] Guang-Ming Zhang, Yi-feng Yang, and Fu-Chun Zhang, "Self-doped Mott insulator for parent compounds of nickelate superconductors," Phys. Rev. B **101**, 020501(R) (2020).
[38] Zhan Wang, Guang-Ming Zhang, Yi-feng Yang, and Fu-Chun Zhang, "Distinct pairing symmetries of superconductivity in infinite-layer nickelates," Phys. Rev. B **102**, 220501(R) (2020).
[39] Peiheng Jiang, Liang Si, Zhaoliang Liao, and Zhicheng Zhong, "Electronic structure of rare-earth infinite-layer $RNiO_2$ (R = La, Nd)," Phys. Rev. B **100**, 201106(R) (2019).
[40] Liang Si, Wen Xiao, Josef Kaufmann, Jan M. Tomczak, Yi Lu, Zhicheng Zhong, and Karsten Held, "Topotactic Hydrogen in Nickelate Superconductors and Akin Infinite-Layer Oxides ABO_2," Phys. Rev. Lett. **124**, 166402 (2020).
[41] Siheon Ryee, Hongkee Yoon, Taek Jung Kim, Min Yong Jeong, and Myung Joon Han, "Induced magnetic two-dimensionality by hole doping in the superconducting infinite-layer nickelate $Nd_{1-x}Sr_xNiO_2$," Phys. Rev. B **101**, 064513 (2020).
[42] I. Leonov, S. L. Skornyakov, and S. Y. Savrasov, "Lifshitz transition and frustration of magnetic moments in infinite-layer $NdNiO_2$ upon hole doping," Phys. Rev. B **101**, 241108(R) (2020).
[43] Hirofumi Sakakibara, Hidetomo Usui, Katsuhiro Suzuki, Takao Kotani, Hideo Aoki, Kazuhiko Kuroki, "Model Construction and a Possibility of Cupratelike Pairing in a New d^9 Nickelate Superconductor (Nd,Sr)NiO_2," Phys. Rev. Lett. **125**, 077003 (2020).
[44] Priyo Adhikary, Subhadeep Bandyopadhyay, Tanmoy Das, Indra Dasgupta, Tanusri Saha-Dasgupta, "Orbital-selective superconductivity in a two-band model of infinite-layer nickelates," Phys. Rev. B **102**, 100501(R) (2020).
[45] Mi-Young Choi, W. E. Pickett, K.-W. Lee, "Quantum-Fluctuation-Frustrated Flat Band Instabilities in $NdNiO_2$," arXiv:2005.03234 (2020).
[46] Valerio Olevano, Fabio Bernardini, Xavier Blase, Andrés Cano, "Ab initio many-body GW correlations in the electronic structure of $LaNiO_2$," arXiv:2001.09194 (2020).
[47] Benjamin Geisler and Rossitza Pentcheva, "Fundamental difference in the electronic reconstruction of infinite-layer versus perovskite neodymium nickelate films on $SrTiO_3$(001)," Phys. Rev. B **102**, 020502(R) (2010).
[48] Fabio Bernardini and Andres Cano, "Stability and electronic properties of $LaNiO_2/SrTiO_3$ heterostructures," J. Phys. Mater. **3**, 03LT01 (2020).
[49] Jiacheng Gao, Zhijun Wang, Chen Fang, Hongming Weng, "Electronic structures and topological properties in nickelates $Ln_{n+1}Ni_nO_{2n+2}$," National Science Review, nwaa218 (2020).
[50] Antoine Georges, Gabriel Kotliar, Werner Krauth, and Marcelo J. Rozenberg, "Dynamical mean-field theory of strongly correlated fermion systems and the limit of infinite dimensions," Rev. Mod. Phys. **68**, 13 (1996).
[51] G. Kotliar, S. Y. Savrasov, K. Haule, V. S. Oudovenko, O. Parcollet, and C. A. Marianetti, "Electronic structure calculations with dynamical mean-field theory," Rev. Mod. Phys. **78**, 865 (2006).
[52] K. Held, "Electronic structure calculations using dynamical mean field theory," Advances in Physics **56**, 829 (2007).
[53] Kristjan Haule, Chuck-Hou Yee, and Kyoo Kim, "Dynamical mean-field theory within the full-potential methods: Electronic structure of $CeIrIn_5$, $CeCoIn_5$, and $CeRhIn_5$," Phys. Rev. B **81**, 195107 (2010).
[54] Peter Blaha, Karlheinz Schwarz, Fabien Tran, Robert Laskowski, Georg K. H. Madsen, and Laurence D. Marks, "WIEN2k: An APW+lo program for calculating the

properties of solids," J. Chem. Phys. **152**, 074101 (2020).
[55] Kristjan Haule, "Exact Double Counting in Combining the Dynamical Mean Field Theory and the Density Functional Theory," Phys. Rev. Lett. **115**, 196403 (2015).
[56] See Supplemental Material, which includes Refs. [1, 4, 5, 11, 14, 17, 43, 44, 53–55, 58–73], for the computational details, DFT electronic structure, decomposition of the Drude peak, impact of broadening factor on optic calculations, comparison with $NdNiO_2$, optical conductivity for different Coulomb U parameters, comparison with $CaCuO_2$, optics for a prototypical Mott system of V_2O_3, 3-dimensional Fermi surfaces of $La_{1-x}Sr_xNiO_2$ computed with DFT+DMFT, the DMFT valence histogram as a function of Hund's coupling J_H, coherence-incoherence crossover, the two-band model based on the Wannier interpretation, and the dynamical crystal field splitting.
[57] D. N. Basov, Richard D. Averitt, Dirk van der Marel, Martin Dressel, and Kristjan Haule, "Electrodynamics of correlated electron materials," Rev. Mod. Phys. **83**, 471 (2011).
[58] M. M. Qazilbash, J. J. Hamlin, R. E. Baumbach, Lijun Zhang, D. J. Singh, M. B. Maple, and D. N. Basov, "Electronic correlations in the iron pnictides," Nature Physics **5**, 647 (2009).
[59] Xiaoyu Deng, Aaron Sternbach, Kristjan Haule, D. N. Basov, and Gabriel Kotliar, "Shining Light on Transition-Metal Oxides: Unveiling the Hidden Fermi Liquid," Phys. Rev. Lett. **113**, 246404 (2014).
[60] Philipp Werner, Armin Comanac, Luca de' Medici, Matthias Troyer, and Andrew J. Millis, "Continuous-Time Solver for Quantum Impurity Models," Phys. Rev. Lett. **97**, 076405 (2006).
[61] Kristjan Haule, "Quantum Monte Carlo impurity solver for cluster dynamical mean-field theory and electronic structure calculations with adjustable cluster base," Phys. Rev. B **75**, 155113 (2007).
[62] John P. Perdew, Kieron Burke, and Matthias Ernzerhof, "Generalized Gradient Approximation Made Simple," Phys. Rev. Lett. **77**, 3865 (1996).
[63] Mark Jarrell, J. E. Gubernatis, "Bayesian inference and the analytic continuation of imaginary-time quantum Monte Carlo data," Physics Reports **269**, 133 (1996).
[64] Arash A. Mostofi, Jonathan R. Yates, Young-Su Lee, Ivo Souza, David Vanderbilt, Nicola Marzari, "wannier90: A tool for obtaining maximally-localised Wannier functions," Computer Physics Communications **178**, 685 (2008).
[65] Giovanni Pizzi *et al.*, "Wannier90 as a community code: new features and applications," J. Phys.: Condens. Matter **32**, 165902 (2020).
[66] Mi-Young Choi, Kwan-Woo Lee, and Warren E. Pickett, "Role of $4f$ states in infinite-layer $NdNiO_2$" Phys. Rev. B **101**, 020503(R) (2020).
[67] Xiangang Wan, Vsevolod Ivanov, Giacomo Resta, Ivan Leonov, Sergey Y. Savrasov, "Calculated Exchange Interactions and Competing $S = 0$ and $S = 1$ States in Doped $NdNiO_2$" arXiv:2008.07465 (2020).
[68] K. Haule and G. Kotliar, "Coherence-incoherence crossover in the normal state of iron oxypnictides and importance of Hund's rule coupling," New J. Phys. **11**, 025021 (2009).
[69] Jernej Mravlje, Markus Aichhorn, Takashi Miyake, Kristjan Haule, Gabriel Kotliar, and Antoine Georges, "Coherence-Incoherence Crossover and the Mass-Renormalization Puzzles in Sr_2RuO_4," Phys. Rev. Lett. **106**, 096401 (2011).
[70] Jernej Mravlje and Antoine Georges, "Thermopower and Entropy: Lessons from Sr_2RuO_4," Phys. Rev. Lett. **117**, 036401 (2016).
[71] F. Hardy, A. E. Böhmer, D. Aoki, P. Burger, T. Wolf, P. Schweiss, R. Heid, P. Adelmann, Y. X. Yao, G. Kotliar, J. Schmalian, and C. Meingast, "Evidence of Strong Correlations and Coherence-Incoherence Crossover in the Iron Pnictide Superconductor KFe_2As_2," Phys. Rev. Lett. **111**, 027002 (2013).
[72] H. Miao, Z. P. Yin, S. F. Wu, J. M. Li, J. Ma, B.-Q. Lv, X. P. Wang, T. Qian, P. Richard, L.-Y. Xing, X.-C. Wang, C. Q. Jin, K. Haule, G. Kotliar, and H. Ding, "Orbital-differentiated coherence-incoherence crossover identified by photoemisson spectroscopy in LiFeAs," Phys. Rev. B **94**, 201109(R) (2016).
[73] Z. K. Liu, M. Yi, Y. Zhang, J. Hu, R. Yu, J.-X. Zhu, R.-H. He, Y. L. Chen, M. Hashimoto, R. G. Moore, S.-K. Mo, Z. Hussain, Q. Si, Z. Q. Mao, D. H. Lu, and Z.-X. Shen, "Experimental observation of incoherent-coherent crossover and orbital-dependent band renormalization in iron chalcogenide superconductors," Phys. Rev. B **92**, 235138 (2015).
[74] A. A. Schafgans, S. J. Moon, B. C. Pursley, A. D. LaForge, M. M. Qazilbash, A. S. Sefat, D. Mandrus, K. Haule, G. Kotliar, and D. N. Basov, "Electronic Correlations and Unconventional Spectral Weight Transfrer in the High-Temperature Pnictide $BaFe_{2-x}Co_xAs_2$ Superconductor Using Infrared Spectroscopy," Phys. Rev. Lett. **108**, 147002 (2012).
[75] To provide an additional test for the Hund's character of the $LaNiO_2$ system, we investigate the Coulomb parameter U dependence of the optical conductivity (see Section VI in Supplemental Material [56]). Increasing U just reduces the overall magnitude of the optical conductivity (since U suppresses the charge fluctuations) but does not affect all the interesting spectral weight transfer effects as a function of temperature and doping which are the signatures of the Hund's metal.
[76] Z is estimated from $1/Z = 1-\partial \mathrm{Im}\Sigma(i\omega)/\partial\omega|_{\omega\to 0^+}$ and it is comparable to the result from analytical continuation of the modified Gaussian method.
[77] Xiaoyu Deng, Jernej Mravlje, Rok Žitko, Michel Ferrero, Gabriel Kotliar, and Antoine Georges, "How Bad Metals Turn Good: Spectroscopic Signatures of Resilient Quasiparticles," Phys. Rev. Lett. **110**, 086401 (2013).
[78] Wenhu Xu, Kristjan Haule, and Gabriel Kotliar, "Hidden Fermi Liquid, Scattering Rate Saturation, and Nernst Effect: A Dynamical Mean-Field Theory Perspective," Phys. Rev. Lett. **111**, 036401 (2013).
[79] Xiaoyu Deng, Kristjan Haule, and Gabriel Kotliar, "Transport Properties of Metallic Ruthenates: A DFT + DMFT Investigation," Phys. Rev. Lett. **116**, 256401 (2016).
[80] Masatoshi Imada, Atsushi Fujimori, and Yoshinori Tokura, "Metal-insulator transitions," Rev. Mod. Phys. **70**, 1039 (1998).
[81] n_e for Ni $d_{x^2-y^2}$ changes significantly upon doping, however its high-energy occupation number, that is obtained from integration of the DMFT spectral function $A(\omega)$ up to E_F, is almost constant of ~ 1.20 upon doping.
[82] Electronic structure of an isostructural $CaCuO_2$ is also computed for comparison. From the DMFT valence his-

togram of $CaCuO_2$, Hund's physics is not noticeable in the cuprate while Mott physics is evident therein (see Figs. S9 and S18 in Supplemental Material [56]).

[83] Luca de'Medici, Jernej Mravlje, and Antoine Georges, "Janus-Faced Influence of Hund's Rule Coupling in Strongly Correlated Materials," Phys. Rev. Lett. **107**, 256401 (2011).

[84] Antoine Georges, Luca de' Medici, and Jernej Mravlje, "Strong Correlations from Hund's Coupling," Annual Review of Condenced Matter Physics **4**, 137 (2013).